

pubs.acs.org/JPCL Letter

# Shear Modes in a 2D Polar Metal

Wen He, Maxwell T. Wetherington, Kanchan Ajit Ulman, Jennifer L. Gray, Joshua A. Robinson, and Su Ying Quek\*



Cite This: J. Phys. Chem. Lett. 2022, 13, 4015-4020



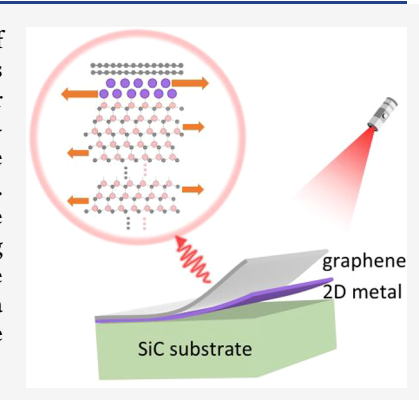
**ACCESS** I

III Metrics & More



Supporting Information

ABSTRACT: Low-frequency shear and breathing modes are important Raman signatures of two-dimensional (2D) materials, providing information on the number of layers and insights into interlayer interactions. We elucidate the nature of low-frequency modes in a 2D polar metal—2D Ga covalently bonded to a SiC substrate, using a first-principles Green's function-based approach. The low-frequency Raman modes are dominated by surface resonance modes, consisting primarily of out-of-phase shear modes in Ga, coupled to SiC phonons. Breathing modes are strongly coupled to the substrate and do not give rise to peaks in the phonon spectra. The highest-frequency shear mode blue-shifts significantly with increasing thickness, reflecting both an increase in the number of Ga layers and an increase in the effective interlayer force constant. The surface resonance modes evolve into localized 2D Ga modes as the phonon momentum increases. The predicted low-frequency modes are consistent with Raman measurements on 2D polar Ga.



etals in the two-dimensional limit have long intrigued etals in the two-universities. Scientists, dating back to studies on two-dimensional electron gases in quantum well structures, where the quantum Hall effect was first demonstrated. Two-dimensional (2D) metallic systems beyond the electron gas have since become experimentally available, such as 2D metals epitaxially grown on substrates<sup>2</sup> and 2D metallic transition metal dichalcogenides, where strong electron-phonon coupling interactions lead to emergent phenomena, such as superconductivity and charge density waves.<sup>3</sup> Environmentally stable, atomically thin 2D polar metals have recently been synthesized by confinement heteroepitaxy approaches. 4,5 These 2D polar metals are covalently bonded to a SiC substrate and are protected by a graphene overlayer which interacts with the metal via van der Waals interactions. This new generation of stable 2D metals significantly expands the scope of interests for 2D metallic systems and are promising for quantum-engineered nanophotonics, on nonlinear optical applications, and superconducting devices.4

The quantum confinement effects in 2D materials can lead to significant changes in properties as a function of thickness.<sup>8,9</sup> Systematic studies to characterize the atomic structure of these 2D polar metals are fundamental for gaining insight into structure-property relationships. Low-frequency interlayer shear and breathing modes provide important Raman signatures that have proven to be particularly useful in providing information on the thickness and stacking order of 2D materials.<sup>10,11</sup> These low-frequency modes also provide experimental insights into the nature and strength of the interlayer interactions in 2D layered materials.<sup>12,13</sup> Low-frequency Raman modes and their thickness dependence are of particular interest in the 2D polar metals, because the range

of interlayer interactions—van der Waals, metallic, and covalent—found in these systems is unprecedented and the influence of these varied interactions on the low-frequency modes is unknown. Furthermore, the influence of substrates on the low-frequency modes in 2D materials has thus far been largely neglected, <sup>10,11</sup> although an ultralow-frequency mode in supported 2D Bi<sub>2</sub>Te<sub>3</sub> was tentatively assigned to a substrate-induced interface mode in one study. <sup>14</sup> The covalent interactions of the 2D polar metals to the SiC substrate<sup>4</sup> provide an excellent opportunity to evaluate the effects of substrates on the low-frequency phonon modes.

In this work, we elucidate the nature of the low-frequency phonon modes in a 2D polar metal, few-layer (1–4 layers) Ga on SiC, using state-of-the-art first-principles calculations. A Green's function approach is employed to account for the semi-infinite nature of the SiC substrate. Our calculations show that close to the Brillouin zone center, the low-frequency phonon modes are surface resonance modes, involving Ga modes coupled to SiC phonons. Interestingly, all the surface resonance modes are shear modes, with out-of-phase shear modes being the most prominent. Away from the zone center, the low-frequency modes become decoupled from the SiC substrate, forming surface localized modes. The highest-frequency shear mode blue-shifts significantly with increasing

Received: March 11, 2022 Accepted: April 19, 2022 Published: April 29, 2022





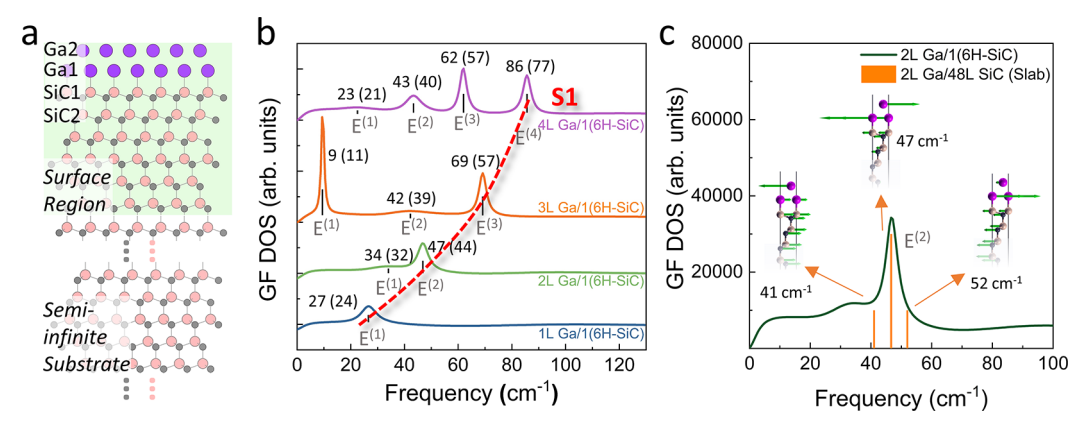


Figure 1. Phonons at  $\Gamma$  point computed by the Green's function approach. (a) Atomic structure of 2L Ga/SiC semi-infinite system. The surface region used in the Green's function approach is indicated in green (see Methods). (b) GF DOS at the zone center for 1L–4L Ga/SiC in the low-frequency region (see Figure S2 for the full frequency range). Lorentzian peaks are labeled by their frequencies in cm<sup>-1</sup>. These numbers are computed using the LDA (PBE) exchange-correlation functionals. Unless otherwise indicated, other figures show results obtained using the LDA exchange-correlation functional. The red dashed line is a guide to the eye showing the thickness-dependent frequency of the highest frequency shear mode S1. The labels, 1–4L Ga/1(6H-SiC), refer to the fact that 1–4L Ga and one 6H-SiC unit (6L SiC) are included in the surface region shown in panel a. (c) Schematic illustrating the phonon mode displacements corresponding to a GF DOS peak with finite width in 2L Ga/SiC. The phonon mode displacements shown here are obtained using a 2L Ga/48L SiC slab model. Purple, light pink, and gray balls refer to Ga, Si, and C atoms, respectively.

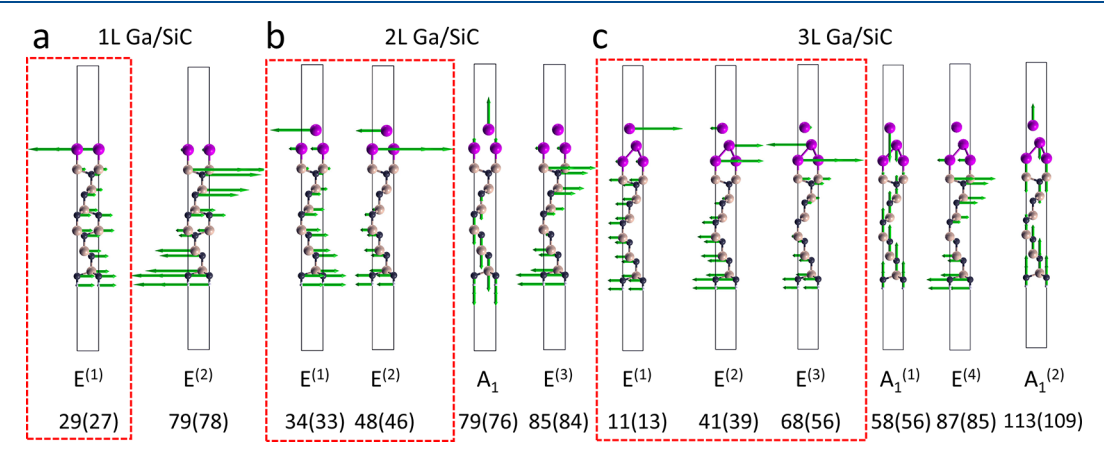


Figure 2. Phonons at  $\Gamma$  point computed by the slab model. (a–c) Atomic displacements of modes with frequencies below 130 cm<sup>-1</sup>, for NL Ga/SiC slabs passivated by hydrogen atoms ((a) 1L, (b) 2L, and (c) 3L). The LDA (PBE) frequencies given below the models are in units of cm<sup>-1</sup>. Phonon displacements of modes for 4L Ga/SiC are given in Figure S4. Red dashed squares highlight the modes that show up as peaks in the GF DOS in Figure 1b.

number of Ga layers. In contrast to layered van der Waals materials, we observe that the effective interlayer force constant within 2D Ga increases with thickness. Raman measurements on the 2D polar Ga on SiC reveal clear peaks that are consistent with our predictions. This work provides fundamental insights into the nature of low-frequency phonon modes in 2D polar metals, and illustrates the impact of substrate-coupling and layer-thickness on the frequencies of these modes.

The atomic structure of 2D Ga on SiC used in this work (e.g., Figure 1a) is consistent with high-resolution high-angle annular dark-field cross-sectional scanning transmission electron microscope (HAADF-STEM) images (Figure S1) and represents the energetically most stable structure according to density functional theory (DFT) calculations. Experimentally, it has been found that the low-frequency Raman spectra are independent of the number of graphene overlayers on top of 2D Ga. 15 Our DFT calculations also show that the graphene shear and breathing modes are essentially

decoupled from the Ga and SiC phonons (Table S1). Similarly, graphene electronic states are decoupled from those of Ga and SiC. <sup>4,5</sup> As such, the results presented here are obtained without graphene overlayers.

In contrast to traditional layered van der Waals materials, 2D Ga is strongly coupled to the covalent SiC substrate. To simulate the phonons in the surface region corresponding to 2D Ga, we adopt a first-principles Green's function (GF) approach (see Methods) to compute the phonon density of states (DOS) for phonons with specific wave vectors. The GF DOS is computed for atoms in the surface region (indicated in green in Figure 1a), taking into account semi-infinite boundary conditions for SiC using a self-energy term. Figure 1b shows the GF DOS for 1L-4L Ga/SiC for phonons at the zone center ( $\Gamma$ ) in the low-frequency range. Lorentzian peaks, which are absent from the GF DOS of the bare SiC substrate (Figure S2), are present below 130 cm<sup>-1</sup>. Including more SiC layers in the surface region (Figure 1a) does not change the energies of these peaks, or the number of peaks in the DOS (Figure S3).

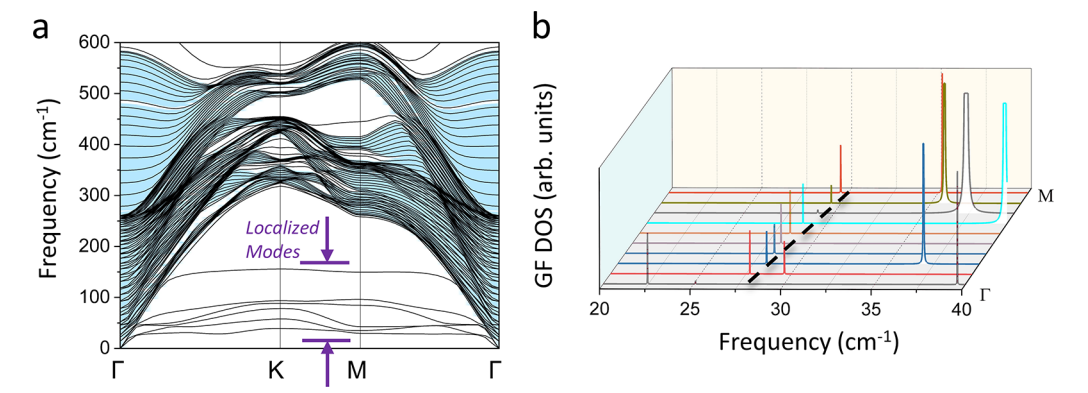


Figure 3. Phonon dispersion and off-Γ GF DOS of 2L Ga/SiC system. (a) Phonon dispersion (black lines) of 2L Ga/30 L SiC superposed with the surface-projected bulk phonon bands of SiC (blue shaded area) below 600 cm<sup>-1</sup>. (b) GF DOS of 2L Ga/SiC system at off-Γ q-points (the GF DOS at Γ point is not plotted) along high symmetry path Γ-M. The evolution of one mode at ~28–29 cm<sup>-1</sup> is marked by the black dashed line. See Figure S6 for GF DOS of 2L Ga/SiC system along Γ-K.

The finite peak widths indicate that these Ga phonon modes are coupled to SiC substrate modes (see Figure 1c), resulting in a frequency broadening. These modes are surface resonance modes <sup>16</sup>—the phonon eigenstates involve both Ga and SiC atoms, but the displacements of Ga atoms are larger compared to those of SiC.

It is instructive to compare peak positions in Figure 1b with phonon frequencies obtained from conventional slab calculations. Figure 2a-c shows the phonon displacements and frequencies for 1L-3L Ga on a hydrogen-terminated, six-layer SiC slab, for  $\Gamma$ -point modes with frequencies below 130 cm<sup>-1</sup> (see Figure S4 for 4L Ga). There are more modes in the slab models than there are peaks in the GF DOS, and the number of these modes increases with increasing slab thickness. The GF approach accounts for a semi-infinite substrate. For surface resonance modes, the SiC substrate modes couple to the surface Ga mode to form a frequency continuum, resulting in a peak in the GF DOS (Figure 1c). Furthermore, taking 2L Ga/ SiC as an example, it is clear that the phonon frequencies are sensitive to the number of SiC layers in the slab model (Figure S5). Despite the challenges in interpreting the calculations from the slab models, it is still possible to use the slab models to assign the peaks in the GF DOS. In particular, the modes closest in frequency to the peaks in the GF DOS are less sensitive to the thickness of the SiC slab in the slab models (see, for instance, the data for mode E<sup>(2)</sup> in 2LGa/SiC in Figure S5). Such modes are marked with dashed red boxes in Figure 2. Interestingly, all these modes are interlayer Ga shear modes, coupled with SiC phonons. In contrast to the shear modes in layered van der Waals materials, there is a clear asymmetry in the atomic displacements because of the strong coupling to the substrate, as well as asymmetric interlayer distances (Table S2).

It can be observed that *N* peaks are observed in the GF DOS for *N*L Ga/SiC (Figure 1b). The GF DOS for 1L Ga/SiC has one peak at 27 cm<sup>-1</sup>; that for 2L Ga/SiC has a peak at 47 cm<sup>-1</sup> and a broad feature at 34 cm<sup>-1</sup>; that for 3L Ga/SiC has three peaks in the GF DOS, including one broad feature at 42 cm<sup>-1</sup>, and two sharper peaks at 9 and 69 cm<sup>-1</sup>. Moreover, the GF DOS for 4L Ga/SiC exhibits one broad feature at 23 cm<sup>-1</sup> and three sharper peaks at 43, 62, and 86 cm<sup>-1</sup>. The broad features correspond to modes that are more strongly coupled to the substrate.

From the symmetry of the point group  $(C_{3\nu})$ , there are (N-1) doubly degenerate interlayer in-plane shear modes (E) and (N-1) interlayer out-of-plane breathing modes  $(A_1)$  in isolated N L Ga. The N peaks in the GF DOS correspond to N shear modes, including the in-plane acoustic modes in isolated Ga, which have nonzero frequencies due to interactions with the substrate. None of the breathing modes show up as peaks in the GF DOS, indicating that they are more strongly coupled to the SiC substrate than the shear modes. Modes that are predominantly attributed to SiC atoms (e.g., E<sup>(3)</sup> in 2L Ga/ SiC; see Figure 2) also do not feature in the GF DOS. The broad features for 2L, 3L, and 4L Ga/SiC correspond to modes in which the vibrations of different Ga atoms are mostly in-phase ( $E^{(1)}$  in 2L and 4L Ga/SiC,  $E^{(2)}$  in 3L Ga/SiC). In these modes, the maximum magnitude of atomic displacements for Si and C are comparable to those for Ga. In contrast, the sharper peaks in the GF DOS arise from out-of-phase Ga shear modes, with larger atomic displacements in Ga relative to those in Si and C atoms.

The shear modes with the highest frequency (S1 in Figure 1b) correspond to modes where atomic displacements in adjacent Ga layers are all out-of-phase. Their phonon eigenvectors are illustrated by  $E^{(1)}$  in 1L Ga/SiC,  $E^{(2)}$  in 2L Ga/SiC, E<sup>(3)</sup> in 3L Ga/SiC, and E<sup>(4)</sup> in 4L Ga/SiC in Figures 2a-c and S4. S1 blue-shifts as the number of Ga layers, N, increases. This trend is similar to that for the highest frequency shear modes in van der Waals layered materials, 17,18 where the blue-shift was explained quantitatively by a simple linear chain model with a fixed interlayer force constant; increasing N results in a stronger restoring force associated with more outof-phase displacements between adjacent layers, each layer constituting one unit of the linear chain. However, for 2D polar Ga, the effective interlayer force constants in Ga also increase with increasing N, resulting in an even more pronounced increase in frequency as N increases (see section S1). This observation is consistent with the average decrease in interlayer distances with increasing N (Table S2).

While the phonon modes at  $\Gamma$  are most relevant for Raman scattering, disorder in the atomic structure or the presence of domains can induce Raman scattering from off- $\Gamma$  phonons. From a fundamental point of view, it is also interesting to investigate the evolution of the phonon frequencies with wavevector within the Brillouin zone. Figure 3a shows the phonon dispersion of a 2L Ga/30L SiC slab, superposed on the surface-

projected bulk phonon bands of 6H-SiC (see section S2). Phonon branches that overlap with the surface-projected bulk phonons of 6H-SiC correspond to either SiC modes or surface resonance modes. As the phonon wave-vector increases in magnitude, the surface resonance modes at  $\Gamma$  evolve into surface localized modes (Figure 3a), which show up as delta-function-like peaks in the GF DOS (Figure 3b).

Figure 4 shows the experimental Raman spectra for 2D Ga/SiC in two regions of the sample, obtained using 633 nm

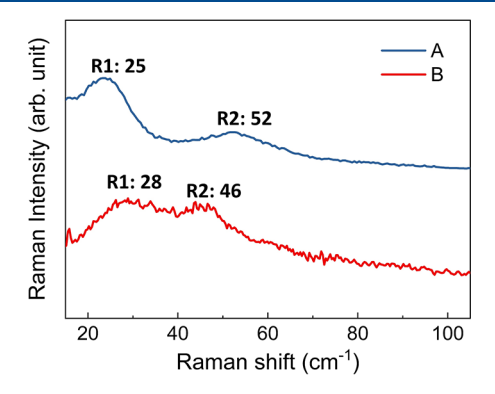


**Figure 4.** Experimental Raman spectra of 2D Ga. Raman spectra of 2D Ga in regions A and B under a 633 nm laser. R1 and R2 are two obvious Raman signals observed in the experimental Raman spectra. Their frequencies are labeled in cm<sup>-1</sup>. The Raman spectra are normalized to the folded transverse optical (FTO) mode of 6H-SiC at 789 cm<sup>-1</sup>. See Table S3 for details of regions A and B.

incident light. Both regions are dominated by a combination of 1-3L Ga, according to cross-sectional HAADF-STEM images (Table S3). The peaks, R1 (A:  $\sim$ 25 cm<sup>-1</sup>, B:  $\sim$ 28 cm<sup>-1</sup>) and R2 (A:  $\sim$ 52 cm<sup>-1</sup>, B:  $\sim$ 46 cm<sup>-1</sup>), are close in frequency to the most prominent low-frequency peaks observed in the GF DOS for zone-center phonons in 1–2L Ga on SiC (Figure 1b;  $E^{(1)}$ in 1L: 27 cm<sup>-1</sup>,  $E^{(2)}$  in 2L: 47 cm<sup>-1</sup>). The broad features in the GF DOS ( $E^{(1)}$  in 2L and  $E^{(2)}$  in 3L) may also contribute to the observed Raman signals, due to resonant enhancement effects (unpublished results). E<sup>(3)</sup> in 3L Ga/SiC is not observed in experiment; our calculations on resonant Raman intensities confirm that this shear mode has a significantly lower Raman intensity at 633 nm (unpublished results). We have also performed Raman measurements with cross- and parallelpolarization configurations. The R1 and R2 peaks are observed under both configurations (Figure S7), confirming that these peaks correspond to shear modes rather than breathing modes.<sup>18</sup> Taken together, the experimental measurements clearly demonstrate the observation of the predicted lowfrequency interlayer shear modes in 2D polar Ga, and constitute the first reports of shear modes in a 2D metal. We further comment that scattering lengths of  $\sim 1$  nm also result in a phonon peak at  $\sim$ 27 cm<sup>-1</sup>, and this corresponds to an inplane longitudinal acoustic mode (Figure S8). This short wavelength scattering may not be relevant given the domain sizes of ~10-70 nm observed here (Table S3) but can be important in 2D alloys.<sup>5</sup>

In conclusion, we have elucidated the nature of low-frequency phonons in a 2D polar metal—2D Ga on SiC. Surface resonance modes with in-plane shear vibrations are predicted and observed in Raman experiments. Thickness-dependent phonon frequencies reveal that the effective interlayer force constant within the 2D metal increases as the

thickness increases from 1L to 4L. This observation is distinct from that in van der Waals layered materials, and arises from the coupling of the 2D metal to the substrate, which results in an asymmetric bonding profile in the system. We expect that the low-frequency shear modes predicted here will also be present in other 2D metals (e.g., In, Ag, alloys)<sup>15</sup> that have similarly been fabricated by heteroepitaxy on SiC. A clear understanding of the low-frequency phonon modes in these 2D polar metals is important for developing an atomic-scale understanding of the coherent, coupled electron and phonon dynamics in these emerging systems.<sup>19</sup>

### METHODS

**Green's Function Method.** The Green's function  $\tilde{G}$  corresponding to the dynamical matrix of a system is given by

$$(\epsilon I - D)\tilde{G} = I \tag{1}$$

where  $\epsilon = (\omega + i\eta)^2$ ,  $\eta$  is a positive infinitesimal number  $0^+$ , I is the identity matrix, D is the dynamical matrix, and  $\tilde{G}$  is the Green's function matrix of the whole system.  $\tilde{G}$  can be partitioned according to individual parts.

2D metal/SiC systems are semi-infinite as illustrated in Figure 1a. Hence, the dynamical matrix in eq 1 is a semi-infinite matrix. The Green's function  $\tilde{G}$  can be partitioned into submatrices as follows

$$\tilde{G} = \begin{bmatrix} G_{S} & G_{SB} \\ G_{BS} & G_{B} \end{bmatrix} = \begin{bmatrix} (\epsilon I_{s} - D_{S}) & d_{SB} \\ d_{SB}^{\dagger} & (\epsilon I_{B} - D_{B}) \end{bmatrix}^{-1}$$
(2)

where the matrix  $(\epsilon I_s - D_S)$  corresponds to the surface region,  $(\epsilon I_B - D_B)$  is a semi-infinite matrix of the substrate, and  $d_{SB}$  and  $d_{SB}^{\dagger}$  († represents conjugate transpose) are the coupling matrices which take into account interactions between the surface region and the substrate. We include interactions between all atoms in the surface region, and those in the top six layers of SiC, which is one unit of 6H-SiC in the bulk.

The retarded Green's function of the surface region can be expressed explicitly as

$$G_{S} = (\epsilon I_{S} - D_{S} - \Sigma)^{-1}$$
(3)

where  $\Sigma = d_{\rm SB}Gd_{\rm SB}^{\dagger}$  is the self-energy term. G is the so-called uncoupled Green's function of the substrate<sup>20</sup> (see section S2). The self-energy  $\Sigma$  is calculated by an iterative procedure<sup>21,22</sup> as discussed in the section S2.

The spectral function of the surface region is given by

$$A(\omega) = i(G_{\rm S} - G_{\rm S}^{\dagger}) \tag{4}$$

and the density-of-states (DOS) is given by

$$DOS(\omega) = \omega Tr(A(\omega))/\pi \tag{5}$$

The DOS defined here is the GF DOS in the main text.  $\eta$  is  $1E^{-8}$  in our calculations. During the calculations, a simple sumrule is applied to the force constant matrices used to construct the dynamical matrices (see section S3).

**First-Principles Calculations.** DFT calculations are performed using the local density approximation (LDA)<sup>23</sup> and generalized gradient approximation (GGA)<sup>24</sup> for the exchange-correlation functional as implemented in the planewave pseudopotential code, QUANTUM ESPRESSO.<sup>25</sup> The force constant matrices are obtained using density functional perturbation theory (DFPT). See section S4 for details.

**Raman Spectroscopy.** Raman characterization is performed on a Horiba LabRam HR Evolution system, using a gas HeNe 633 nm laser (ThorLabs, HRP350-EC) accompanied by a Volume Bragg Grating notch filter (referred to as ULF filters by Horiba). The spectra are normalized to the FTO mode maximum of the 6H-SiC (789 cm<sup>-1</sup>), and then, a baseline offset is applied. See section S5 for more details.

**Cross-Sectional HAADF-STEM.** Cross-sectional samples for STEM imaging were prepared using the in situ lift-out method in a FEI Helios NanoLab DualBeam 660 focused ion beam (FIB). Cross sections were prepared using the FIB Ga<sup>+</sup> ion beam at 30 kV, and then stepped down to 1 kV to avoid ion beam damage to the sample surface during final thinning. High-resolution STEM imaging of the prepared cross sections was performed in a FEI Titan G2 80–300 transmission electron microscope. See section S6 for details of the microscope and detectors.

#### ASSOCIATED CONTENT

### Supporting Information

The Supporting Information is available free of charge at https://pubs.acs.org/doi/10.1021/acs.jpclett.2c00719.

Cross-sectional HAADF-STEM images, GF DOS in a larger frequency range, GF DOS for different thickness of SiC in the surface region, atomic vibrations of 4L Ga/SiC, phonon frequencies of 2L Ga on SiC with different thickness computed by the slab models, GF DOS at off- $\Gamma$  q-points along  $\Gamma$ -K direction, polarized Raman spectra, GF DOS at off- $\Gamma$  q-points corresponding to domain sizes, analysis of vibrations of graphene overlayers on Ga/SiC, structural parameters, statistical analysis of cross-sectional HAADF-STEM images, linear-chain model, details of the calculation of the self-energy term, sum rule, first-principles calculations, and Raman spectroscopy (PDF)

#### AUTHOR INFORMATION

### **Corresponding Author**

Su Ying Quek — Department of Physics, National University of Singapore, Singapore 117551; Centre for Advanced 2D Materials, National University of Singapore, Singapore 117546; Department of Materials Science and Engineering, National University of Singapore, Singapore 117575; NUS Graduate School Integrative Sciences and Engineering Programme, National University of Singapore, Singapore 117456; orcid.org/0000-0003-4223-2953; Email: phyqsy@nus.edu.sg

#### **Authors**

Wen He — Department of Materials Science and Engineering, National University of Singapore, Singapore 117575; Centre for Advanced 2D Materials, National University of Singapore, Singapore 117546; Present Address: Department of Physics, National University of Singapore, Singapore 117551; orcid.org/0000-0001-7972-8667

Maxwell T. Wetherington — Department of Materials Science and Engineering, The Pennsylvania State University, University Park, Pennsylvania 16802, United States; Materials Research Institute, The Pennsylvania State University, University Park, Pennsylvania 16802, United States Kanchan Ajit Ulman — Centre for Advanced 2D Materials, National University of Singapore, Singapore 117546; orcid.org/0000-0002-5434-6563

Jennifer L. Gray – Materials Research Institute, The Pennsylvania State University, University Park, Pennsylvania 16802, United States

Joshua A. Robinson — Department of Materials Science and Engineering, The Pennsylvania State University, University Park, Pennsylvania 16802, United States; Materials Research Institute, The Pennsylvania State University, University Park, Pennsylvania 16802, United States; Center for 2-Dimensional and Layered Materials, The Pennsylvania State University, University Park, Pennsylvania 16802, United States; 2-Dimensional Crystal Consortium, The Pennsylvania State University, University Park, Pennsylvania 16802, United States; Occid.org/0000-0002-1513-7187

Complete contact information is available at: https://pubs.acs.org/10.1021/acs.jpclett.2c00719

#### Notes

The authors declare no competing financial interest.

#### ACKNOWLEDGMENTS

W.H., K.A.U., and S.Y.Q. acknowledge funding from Grants MOE2016-T2-2-132, MOE2017-T2-2-139, and MOE2018-T3-1-005 from the Ministry of Education (MOE), Singapore, funding from the MOE Research Scholarship Block, and funding from the Singapore National Research Foundation, Prime Minister's Office, under its medium-sized center program. Computations were performed on the NUS Graphene Research Centre cluster and National Supercomputing Centre Singapore (NSCC). J.A.R and M.T.W are supported in-part by Horiba and the Penn State Center for Nanoscale Science through the National Science Foundation Grant DMR-2011839. We thank Yuanxi Wang and Vincent Crespi for discussions.

# **■** REFERENCES

- (1) Von Klitzing, K. The Quantized Hall Effect. Rev. Mod. Phys. 1986, 58 (3), 519-531.
- (2) Wang, T.; Park, M.; Yu, Q.; Zhang, J.; Yang, Y. Stability and Synthesis of 2D Metals and Alloys: A Review. *Mater. Today Adv.* **2020**, *8*, 100092.
- (3) Han, G. H.; Duong, D. L.; Keum, D. H.; Yun, S. J.; Lee, Y. H. Van Der Waals Metallic Transition Metal Dichalcogenides. *Chem. Rev.* **2018**, *118* (13), *6297*–*6336*.
- (4) Briggs, N.; Bersch, B.; Wang, Y.; Jiang, J.; Koch, R. J.; Nayir, N.; Wang, K.; Kolmer, M.; Ko, W.; De La Fuente Duran, A.; et al. Atomically Thin Half-van Der Waals Metals Enabled by Confinement Heteroepitaxy. *Nat. Mater.* **2020**, *19* (6), 637–643.
- (5) Rajabpour, S.; Vera, A.; He, W.; Katz, B. N.; Koch, R. J.; Lassaunière, M.; Chen, X.; Li, C.; Nisi, K.; El-Sherif, H.; et al. Tunable 2D Group-III Metal Alloys. *Adv. Mater.* **2021**, 33, 2104265.
- (6) Nisi, K.; Subramanian, S.; He, W.; Ulman, K. A.; El-Sherif, H.; Sigger, F.; Lassaunière, M.; Wetherington, M. T.; Briggs, N.; Gray, J.; et al. Light–Matter Interaction in Quantum Confined 2D Polar Metals. *Adv. Funct. Mater.* **2021**, *31*, 2005977.
- (7) Steves, M. A.; Wang, Y.; Briggs, N.; Zhao, T.; El-Sherif, H.; Bersch, B. M.; Subramanian, S.; Dong, C.; Bowen, T.; Fuente Duran, A. D. L.; et al. Unexpected Near-Infrared to Visible Nonlinear Optical Properties from 2-D Polar Metals. *Nano Lett.* **2020**, *20* (11), 8312–8318.
- (8) Gupta, A.; Sakthivel, T.; Seal, S. Recent Development in 2D Materials Beyond Graphene. *Prog. Mater. Sci.* **2015**, *73*, 44–126.

- (9) Li, X.-L.; Han, W.-P.; Wu, J.-B.; Qiao, X.-F.; Zhang, J.; Tan, P.-H. Layer-number Dependent Optical Properties of 2D Materials and Their Application for Thickness Determination. Adv. Funct. Mater. 2017, 27 (19), 1604468.
- (10) Lu, X.; Luo, X.; Zhang, J.; Quek, S. Y.; Xiong, Q. Lattice Vibrations and Raman Scattering in Two-dimensional Layered Materials Beyond Graphene. Nano Res. 2016, 9 (12), 3559-3597.
- (11) Liang, L.; Zhang, J.; Sumpter, B. G.; Tan, Q.-H.; Tan, P.-H.; Meunier, V. Low-frequency Shear and Layer-breathing Modes in Raman Scattering of Two-Dimensional Materials. ACS Nano 2017, 11 (12), 11777-11802.
- (12) Luo, X.; Lu, X.; Koon, G. K. W.; Castro Neto, A. H.; Özyilmaz, B.; Xiong, Q.; Quek, S. Y. Large Frequency Change with Thickness in Interlayer Breathing Mode - Significant Interlayer Interactions in Few Layer Black Phosphorus. Nano Lett. 2015, 15 (6), 3931-3938.
- (13) Luo, X.; Lu, X.; Cong, C.; Yu, T.; Xiong, Q.; Ying Quek, S. Stacking Sequence Determines Raman Intensities of Observed Interlayer Shear Modes in 2D Layered Materials - A General Bond Polarizability Model. Sci. Rep. 2015, 5 (1), 14565.
- (14) Zhao, Y.; Luo, X.; Zhang, J.; Wu, J.; Bai, X.; Wang, M.; Jia, J.; Peng, H.; Liu, Z.; Quek, S. Y.; et al. Interlayer Vibrational Modes in Few-quintuple-layer Bi<sub>2</sub>Te<sub>3</sub> and Bi<sub>2</sub>Se<sub>3</sub> Two-dimensional Crystals: Raman Spectroscopy and First-principles Studies. Phys. Rev. B 2014, 90 (24), 245428.
- (15) Wetherington, M. T.; Turker, F.; Bowen, T.; Vera, A.; Rajabpour, S.; Briggs, N.; Subramanian, S.; Maloney, A.; Robinson, J. A. 2-dimensional Polar Metals: A Low-frequency Raman Scattering Study. 2d Mater. 2021, 8 (4), 041003.
- (16) Benedek, G.; Miglio, L. The Green's Function Method in the Surface Lattice Dynamics of Ionic Crystals. In Surface Phonons; Kress, W., de Wette, F. W., Eds.; Springer Series in Surface Sciences, Vol. 21; Springer: Berlin, 1991; pp 37-66.
- (17) Tan, P. H.; Han, W. P.; Zhao, W. J.; Wu, Z. H.; Chang, K.; Wang, H.; Wang, Y. F.; Bonini, N.; Marzari, N.; Pugno, N.; et al. The Shear Mode of Multilayer Graphene. Nat. Mater. 2012, 11 (4), 294-300.
- (18) Zhao, Y.; Luo, X.; Li, H.; Zhang, J.; Araujo, P. T.; Gan, C. K.; Wu, J.; Zhang, H.; Quek, S. Y.; Dresselhaus, M. S.; et al. Interlayer Breathing and Shear Modes in Few-trilayer MoS2 and WSe2. Nano Lett. 2013, 13 (3), 1007-1015.
- (19) Steves, M. A.; Rajabpour, S.; Wang, K.; Dong, C.; He, W.; Quek, S. Y.; Robinson, J. A.; Knappenberger, K. L. Atomic-level Structure Determines Electron-phonon Scattering Rates in 2-D Polar Metal Heterostructures. ACS Nano 2021, 15 (11), 17780-17789.
- (20) Sadasivam, S.; Che, Y.; Huang, Z.; Chen, L.; Kumar, S.; Fisher, T. S. The Atomistic Green's function Method for Interfacial Phonon Transport. Annu. rev. heat transf. 2014, 17, 89-145.
- (21) Sancho, M. P. L.; Sancho, J. M. L.; Sancho, J. M. L.; Rubio, J. Highly Convergent Schemes for the Calculation of Bulk and Surface Green Functions. J. Phys. F: Met. Phys. 1985, 15 (4), 851-858.
- (22) Nardelli, M. B. Electronic Transport in Extended Systems: Application to Carbon Nanotubes. Phys. Rev. B 1999, 60 (11), 7828-7833.
- (23) Perdew, J. P.; Wang, Y. Accurate and Simple Analytic Representation of the Electron-gas Correlation Energy. Phys. Rev. B **1992**, 45 (23), 13244–13249.
- (24) Perdew, J. P.; Burke, K.; Ernzerhof, M. Generalized Gradient Approximation Made Simple. Phys. Rev. Lett. 1996, 77 (18), 3865-
- (25) Giannozzi, P.; Baroni, S.; Bonini, N.; Calandra, M.; Car, R.; Cavazzoni, C.; Ceresoli, D.; Chiarotti, G. L.; Cococcioni, M.; Dabo, I.; et al. QUANTUM ESPRESSO: A Modular and Open-source Software Project for Quantum Simulations of Materials. J. Condens. Matter Phys. 2009, 21 (39), 395502.

# **□** Recommended by ACS

## **Extraordinary Phonon Displacement and Giant Resonance** Raman Enhancement in WSe<sub>2</sub>/WS<sub>2</sub> Moiré Heterostructures

Sharidya Rahman, Yuerui Lu, et al.

NOVEMBER 28, 2022

ACS NANO

READ 2

#### Interlayer Exciton-Phonon Bound State in Bi<sub>2</sub>Se<sub>3</sub>/Monolayer WS, van der Waals Heterostructures

Zachariah Hennighausen, Berend T. Jonker, et al.

JANUARY 16, 2023

ACS NANO

READ **C** 

#### Emergent Moiré Phonons Due to Zone Folding in WSe,-WS, Van der Waals Heterostructures

Hsun-Jen Chuang, Berend T. Jonker, et al.

OCTOBER 12, 2022

ACS NANO

READ **C** 

#### Polarized Moiré Phonon and Strain-Coupled Phonon Renormalization in Twisted Bilayer MoS<sub>2</sub>

Sameer Kumar Mallik, Satyaprakash Sahoo, et al.

SEPTEMBER 07, 2022

THE JOURNAL OF PHYSICAL CHEMISTRY C

READ 2

Get More Suggestions >